Exploring the Design Rules for Efficient Membrane-Reshaping Nanostructures

Joel C. Forster,[1,2,3] Johannes Krausser,[1,2,3] Manish R. Vuyyuru,[1,2] Buzz Baum,[2,3] and Anđela Šarić[1,2,3,*]
[1]Department of Physics and Astronomy, University College London, WC1E 6BS London, United Kingdom
[2]Institute for the Physics of Living Systems, University College London, WC1E 6BS London, United Kingdom
[3]MRC Laboratory for Molecular Cell Biology, University College London, WC1E 6BS London, United Kingdom

(Received 5 March 2020; accepted 6 October 2020; published 23 November 2020)

In this study, we investigate the role of the surface patterning of nanostructures for cell membrane reshaping. To accomplish this, we combine an evolutionary algorithm with coarse-grained molecular dynamics simulations and explore the solution space of ligand patterns on a nanoparticle that promote efficient and reliable cell uptake. Surprisingly, we find that in the regime of low ligand number the best-performing structures are characterized by ligands arranged into long one-dimensional chains that pattern the surface of the particle. We show that these chains of ligands provide particles with high rotational freedom and they lower the free energy barrier for membrane crossing. Our approach reveals a set of nonintuitive design rules that can be used to inform artificial nanoparticle construction and the search for inhibitors of viral entry.

DOI: 10.1103/PhysRevLett.125.228101

Our intuition for how nanostructures in nature operate is guided by experimental observation interpreted through mechanistic models. Such a strategy rests on the researchers' ability to navigate the large phase space of possible models and parameters to capture the key physics behind complex nanoscale phenomena. Here, we take a reverse approach: Rather than deducing the design rules of nanostructures by observing nature, we specify the function that the nanostructure should perform and couple an optimization technique to coarse-grained molecular dynamics (MD) simulations to iterate upon its design.

Such a reverse approach enabled us to uncover design principles of membrane-reshaping nanostructures that we would not have *a priori* postulated based purely on physical intuition or observation. Specifically, we explored the solution space of ligand patterns on a nanoparticle that promote efficient and reliable cell crossing. By observing the structures as their performance improves, we identified nontrivial design rules that aid nanoparticle internalization. We then analyzed the kinetic and thermodynamic features of the well-performing designs to determine the physical mechanisms behind their efficiency.

MD model.—The nanoparticle is modeled as a rigid body, made up of a central particle that carries ligands on its surface which bind to a fluid membrane [Fig. 1(c)]. To curve the membrane and form a vesicle [1,2], a minimal total interaction strength between the ligands and the membrane is required. Importantly, for a given interaction strength, the efficiency of membrane crossing also depends on the ligand arrangement. For instance, if all the ligands are clustered at one pole, the nanoparticle binds strongly but cannot be internalized. To account for different ligand arrangements, the nanoparticle was fully covered by 72 ligand sites, while N of those are active and able to bind to the membrane beads via a Lennard-Jones potential of a depth ϵ [Fig. 1(b)]. The membrane was modeled using a single-particle-thick model [3] that reproduces the mechanical properties of biological membranes and is capable of fission. Simulations were run using Langevin dynamics within LAMMPS [4] (see Methods in Supplemental Material [5]).

Optimization.—To explore efficient nanoparticle designs, we chose an evolutionary algorithm (EA) as an optimization technique due its ease of implementation, efficiency in exploring a large phase space, and ability to trace intermediate solutions. The procedure here starts with a random population of nanostructure designs, then measures how well the individual structures perform a specific task in MD, and finally uses an EA to select, mutate, and breed the fittest members of the population and using the resultant population to repeat the process [Fig. 1(a)]. We kept the total number of active ligands (N) and their binding strength to the membrane (ϵ) constant for each MD or EA instance. The ligand designs were represented by 1D single-bit arrays [Fig. 1(b)], which enabled the following evolutionary algorithm operations: tournament selection, two-point crossover, and shuffling mutation. To avoid premature fixation, the population was split into independent "demes" and permitted to trade individuals every generation [11,12] (see Methods in Supplemental Material [5]).

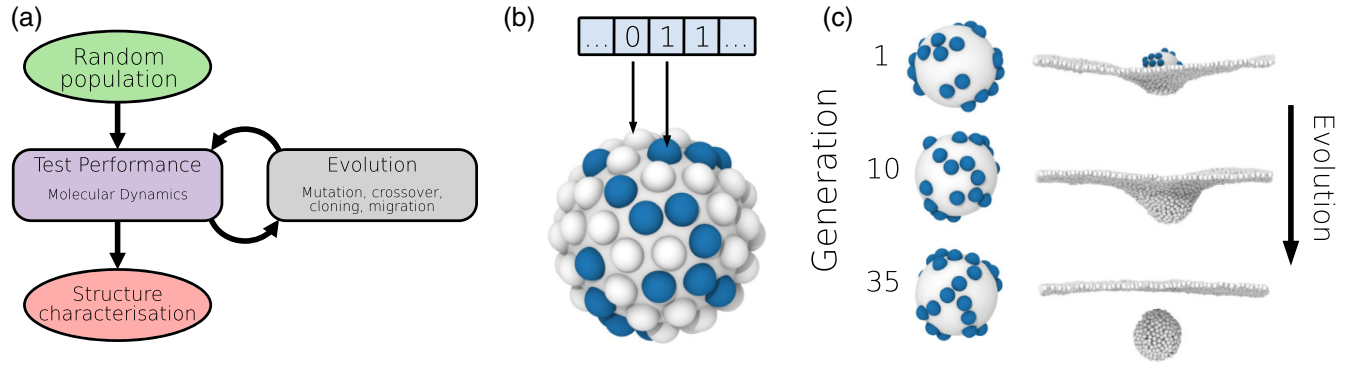

FIG. 1. Combining molecular dynamics and an evolutionary algorithm. (a) Graphical representation of the MD-EA scheme developed here. (b) The nanoparticle is covered by 72 ligands, of which N are active (in blue, represented as "1" in the nanoparticle "genome") and can bind the membrane. (c) Example designs from three different generations along with a snapshot from the last time step of their simulation runs.

As a measurement of the "fitness" of the nanoparticle, we used the degree of its wrapping by the membrane and its speed of membrane crossing:

$$f = \begin{cases} R_c N_c & \text{nonbudding,} \\ R_c N_c + R_t \frac{t_{\text{run}}}{t_b} + R_b & \text{budding,} \end{cases} \quad (1)$$

where N_c is the number of membrane beads in contact with the ligands with a weighting constant R_c. When budding occurred, an additional reward R_b was given. To characterize the efficiency of budding, we measured the time of budding t_b, normalized by the run-time of the total simulation t_{run}, which is equal for all the simulations, and assigned it a weighting constant R_t (see Methods in Supplemental Material [5]).

The evolutionary algorithm was run for 35 generations across four demes, each containing 20 individual particles. Each particle was run under four randomized initial orientations with respect to the membrane plane to ensure the robustness of particle uptake. The average population fitness for a single generation is the average over all 80 individuals and their rotations. This was repeated for different numbers of active ligands ($19 < N < 61$) and ligand-membrane attractions ($3kT < \epsilon < 15kT$), producing a total population of around 1.30×10^6 individuals, with 5.34×10^5 being unique.

Nanoparticle evolution.—Nanoparticle designs in the first generation are typically not able to penetrate the membrane by the end of the MD run, whereas the evolved designs deform the membrane more strongly and eventually bud off [Fig. 1(c)]. Accordingly, the mean fitness of the whole population increases as the evolution progresses and eventually approaches saturation [Fig. 2(a)]. The fitness values are normalized by the mean fitness value of the population of randomly generated particles for the same ϵ and N, $\langle F_r \rangle$, to indicate that the evolved particles outperform the randomly generated ones.

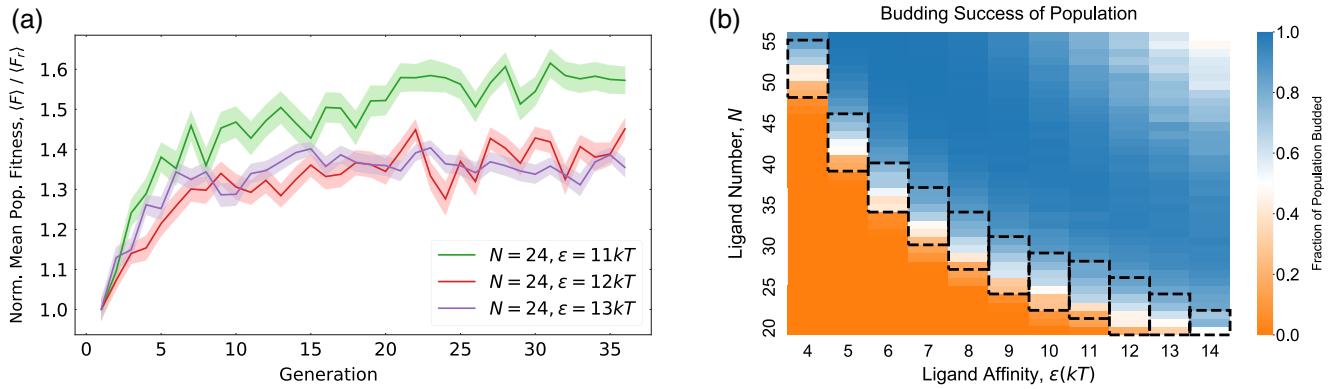

FIG. 2. Performance of the evolved nanoparticles. (a) The normalized population fitness for three examples of the active ligand number N and ligand-membrane interaction ϵ. The error bars represent the standard error of the mean fitness over the population of 80 individuals in one realization of the EA-MD algorithm. Fluctuations in this mean are to be expected, as not all mutations are beneficial. (b) The fraction of the entire population that successfully crossed the membrane at various values of N and ϵ. In the region around $N\epsilon \approx 200kT$ (marked with boxes), the population is made up of a mixed collection of budding and nonbudding particles. In the extreme of very high N and high ϵ, the particle often tears the membrane and simulations cannot be equilibrated (see Supplemental Material [5]).

Figure 2(b) illustrates the average population performance for a wide range of N and ϵ values. For sufficiently large N and ϵ, almost every design will traverse the membrane successfully in the first generation, and in this regime the ligand arrangement is not the deciding factor.

Conversely, for low ligand numbers and low binding strengths, no particle designs can bud in, although their performance can improve with evolutionary time. In the regime of intermediate N and ϵ, the ligand arrangement is crucial for the nanoparticles' budding performance. This is the regime we focus on and define it such that between 15% and 85% of the population penetrated the membrane, which corresponds to the mean total affinity of $N\epsilon = 248.5kT$ and a standard deviation of $28.8kT$ [boxed region in Fig. 2(b)]. We identified 60260 unique particle designs in this region, some of which performed excellently and some very poorly, which points to the importance of the ligands arrangement for efficient budding.

Structural characterization.—The difference between well and poorly performing particles is visible by eye, with the fit particles showing linearly connected ligands, while poorly performing particles have ligands disconnected from each other or highly clustered [Fig. 3(a)]. To objectively characterize nanoparticle designs, we translated the ligand positions on the surface of the particle into nodes of a network. The weights of the edges between the nodes, w, are set to the inverse of the great arc distance between the ligands δ [Fig. 3(b)]. As it uses only pairwise distances, this representation is rotationally invariant. Edges above a threshold of $3.3/\sigma_0$ were removed (σ_0 being the MD unit length), which retains only nearest and next-to-nearest neighbors.

We found that two topological graph properties distinguish between successful and unsuccessful designs: the graph density and the number of disconnected subgraphs. The graph density can be understood as a measure of how clustered and connected the points in the network are. For a particle i, it is defined as $d_i = \{[2|E_i|]/[|V_i|(|V_i|-1)]\} = [(\langle z_i \rangle)/(|V_i|-1)]$, where $|E_i|$ and $|V_i|$ are the number of the particle network's edges and vertices, respectively, and $\langle z_i \rangle$ is the average degree of all nodes in the network.

The number of disconnected subgraphs is the number of separate regions of a graph that share no common nodes; Subgraphs have no connecting edges between them. The population averages of these properties produced the mean density D and subgraph number S of designs at constant N. The same mean can be calculated for random particle designs at constant N, giving D_r and S_r.

Analyzing successful designs.—The average normalized graph density D/D_r and subgraph number S/S_r for the budding and nonbudding population within the critical region from Fig. 2(b) are shown in Fig. 3(c). The main structural difference between the successful and non-successful designs is visible for low and intermediate ligand numbers ($N < 35$), where the number of possible variations in design is the largest. For larger values of N, differences in designs were mostly dependent on the evenness of coverage of the particle. Successful designs ($N < 35$) tend to have lower graph densities, meaning that the ligands have a lower average number of neighbours.

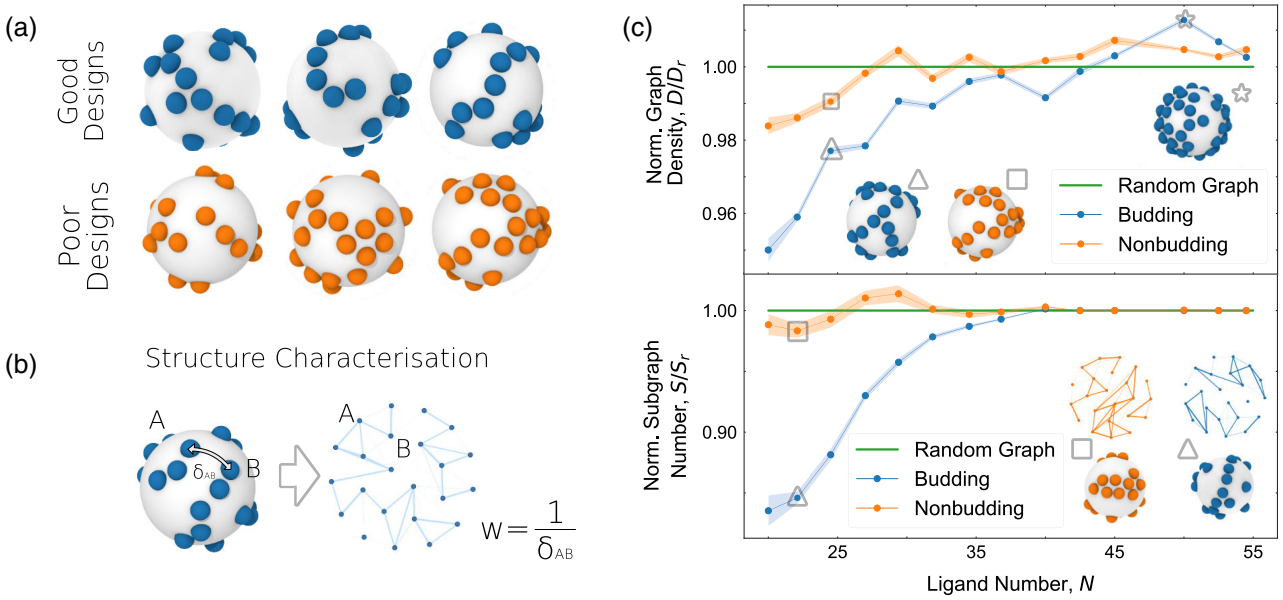

FIG. 3. Structural analysis of the evolved particles. (a) Examples of evolved nanoparticle designs. (b) The patterns of ligands on the particle are converted into a network. (c) The average normalized graph density (upper panel) and the average normalized subgraph size (bottom panel) for the budding and nonbudding particles across the whole population. The insets show sample particles in each subpopulation. The error bars represent the standard error of the mean.

In contrast, such particles also have lower average subgraph numbers. Therefore, ligands in successful particles tend to be connected with one another by only few edges, covering a large angular range across the nanoparticle surface. Taken together, this indicates that successful designs are characterized by patterns in which most ligands are part of the same chainlike subgraph, like those visible in Fig. 3(a) and the inset in Fig. 3(c). Conversely, isolated "patches" of ligands perform very poorly [Fig. 3(a)]. Interestingly, designs that have ligands uniformly distributed across the nanoparticle also show poor performance, with budding times on average 30% longer than that of the evolved successful designs.

We noticed that unsuccessful designs often end up deforming the membrane but never becoming fully wrapped by it. To quantify this behavior, we measured the average rotational mean squared displacement $\Delta\theta^2 = \langle[\theta(\tau) - \theta(0)]^2\rangle$ as particles meet the membrane, bind to it, and deform it across the population of budding and nonbudding particles [Fig. 4(a)]. $\theta(\tau)$ is the angle at time τ between a predefined nanoparticle axis and a predefined vector. While at the beginning of the simulation the rotational displacement does not differ much between budding and nonbudding particles, a significant discrepancy appears prior to budding, where successful particles exhibit substantially larger rotational freedom compared to the nonbudding particles. This freedom enables particles to explore the transitional states needed to be able to wrap themselves in the membrane. Indeed, the frequency of budding events shown in Fig. 4(a) illustrates the direct correlation between rotational rearrangements and successful membrane budding. We also checked the case where rotational displacement is measured only until the point at which a particle buds, as opposed to for its full run length t_{run}, the difference between the budding and nonbudding population remains (Fig. S4 [5]).

Since for fixed N and ϵ all the designs have the same free energy difference between wrapped and nonadsorbed states, the difference in their performances must arise due to different free energy landscapes they experience on the path to full wrapping. Figure 4(b) shows the budding free energy profile for one fit and unfit design, which carry the same total adhesion energy, computed using umbrella sampling with the degree of membrane wrapping as the reaction coordinate. Interestingly, the free energy minimum for the unfit particle is positioned at ~75% membrane wrapping and is separated from the full wrapping by a large barrier. The free energy profile for the fit particle, on the other hand, reaches the global free energy minimum at full wrapping, without encountering any significant energy barriers en route. Taken together, our analysis implies that, by enabling a large coverage of the nanoparticle curvature, the chains of ligands have two roles: (i) to allow for sufficient wrapping and (ii) to guide the rotational rearrangements to efficiently reach full wrapping.

Discussion.—By combining coarse-grained molecular dynamics simulations with evolutionary algorithms, we have been able to evolve nanostructures for a specific function, selected for the ability to bud across the cell membrane. Even in this seemingly simple case, this approach revealed novel design rules that would not have been easy to guess, even for a well-trained modeler. While the evolved designs do not necessarily point to the absolutely optimal ligand patterning for membrane uptake, their shapes do provide new avenues for efficient nanoparticle design. At intermediate and low ligand numbers, the MD-EA scheme identified the nanoparticle designs that have a low free energy barrier for membrane crossing. Such designs are characterized by long chains of ligands, where the chains rarely cross or branch but

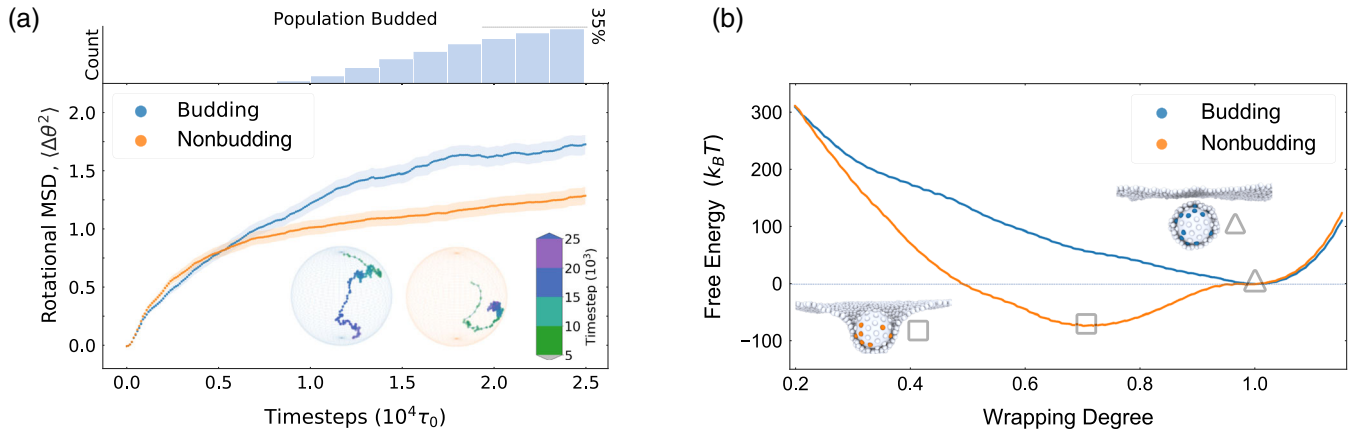

FIG. 4. Explaining successful designs. (a) The rotational mean square displacement of the budding and nonbudding population ($\epsilon = 11kT$, $N = 22$). The error bars represent the standard error of the mean for each subpopulation. The inset shows a sample rotational trajectory for one ligand on one particle from each subpopulation, while the top panel shows the count of the budding events. (b) Free energy as a function of a membrane wrapping for two sample particles from the budding and nonbudding populations ($\epsilon = 11kT$, $N = 22$). The insets show each particle at their free energy minima.

which effectively cover the particle leaving few gaps. Ligand chains minimize the distance between successively adsorbed ligands and guide the membrane wrapping. Chains were often found together with small patches of ligands. While it is possible that such occasional patches have a functional role, this may also be due to the limited number of evolutionary cycles.

The superior performance of some structures is based purely on the kinetics, since the explored designs exist within a small range of total wrapping free energy. Indeed, for any practical application, the rate of membrane crossing is the key factor. We therefore believe that the design rules identified here can aid the design of artificial nanoparticles for cell delivery, as well as possibly explain ligand patterns found in nature. For instance, low-density lipoprotein particles appear to carry membrane-binding proteins arranged into long lines that envelope the particles [13]. Analogously, membrane-binding proteins on some viruses display linear chain arrangements [14–16]. However, unlike in our simulations, biological structures are not necessarily evolved to optimize one well-defined and unique function.

Previous studies incorporated evolutionary strategies within computer simulations mainly for the purpose of energy minimization [17–19] or optimization of interaction parameters [20,21]. Only a few studies used such a combined approach to evolve a structure for a certain function. Kriegman *et al.* [22] used an evolutionary algorithm within a physical engine environment to optimize for organism design of a desired locomotion. At the nanoscale, Srinivasan *et al.* [23] combined an EA with free energy calculations to reverse design sequences on DNA-grafted colloids for a target crystal structure. Miskin and Jaeger [24] combined evolution strategy with MD simulations to evolve a particle shape that produces granular packing of a desired mechanical response, which is the closest in spirit to this study.

While the previous body of work on the subject of nanoparticle uptake identified the importance of the nanoparticle shape [25–27] and ligand distribution [28], each of the studies explored only a small phase space of possible designs (~10). Here we effectively explored tens of thousands of possible unique designs and have identified novel, improved design rules that previous studies did not consider. We envision that the approach developed here can be of great help in identifying the design principles of a range of nanostructures and nanomachines, such as protein filaments, lattices, and other higher-order structures, in the context of both biological and engineered systems.

We acknowledge support from EPSRC (J. C. F.), MRC (B. B. and A. Š.), the ERC StG 802960 "NEPA" (J. K. and A. Š.), the Royal Society (A. Š.), and the United Kingdom Materials and Molecular Modelling Hub for computational resources, which is partially funded by EPSRC (EP/P020194/1).

*a.saric@ucl.ac.uk

[1] H. Gao, W. Shi, and L. B. Freund, Mechanics of receptor-mediated endocytosis, Proc. Natl. Acad. Sci. U.S.A. **102**, 9469 (2005).

[2] T. Curk, P. Wirnsberger, J. Dobnikar, D. Frenkel, and A. Šarić, Controlling cargo trafficking in multicomponent membranes, Nano Lett. **18**, 5350 (2018).

[3] H. Yuan, C. Huang, J. Li, G. Lykotrafitis, and S. Zhang, One-particle-thick, solvent-free, coarse-grained model for biological and biomimetic fluid membranes, Phys. Rev. E **82**, 011905 (2010).

[4] S. Plimpton, A. Thompson, S. Moore, and A. Kohlmeyer, Lammps documentation (2017).

[5] See Supplemental Material at http://link.aps.org/supplemental/10.1103/PhysRevLett.125.228101 for further details on the methods and software used in the study, as well as further discussion of the results and findings. Supplemental Material includes Refs. [6–10].

[6] N. Sloane, Tables of sphere packings and spherical codes, IEEE Trans. Inf. Theory **27**, 327 (1981).

[7] F.-A. Fortin, F.-M. De Rainville, M.-A. Gardner, M. Parizeau, and C. Gagné, DEAP: Evolutionary algorithms made easy, J. Mach. Learn. Res. **13**, 2171 (2012), https://dl.acm.org/doi/10.5555/2503308.2503311.

[8] M. Mitchell, *An Introduction to Genetic Algorithms* (MIT Press, Cambridge, MA, 1998).

[9] D. W. Scott, Kernel density estimation, in *Wiley StatsRef: Statistics Reference Online* (American Cancer Society, Atlanta, 2018), pp. 1–7.

[10] M. Waskom *et al.*, mwaskom/seaborn:v0.8.1 (2017).

[11] M. Affenzeller, S. Winkler, S. Wagner, and A. Beham, *Genetic Algorithms and Genetic Programming: Modern Concepts and Practical Applications*, 1st ed. (Chapman & Hall/CRC, London, 2009).

[12] G. Goos, J. Hartmanis *et al.*, *Lecture Notes in Computer Science* (Springer, New York, 1973).

[13] G. Ren, G. Rudenko, S. J. Ludtke, J. Deisenhofer, W. Chiu, and H. J. Pownall, Model of human low-density lipoprotein and bound receptor based on cryoem, Proc. Natl. Acad. Sci. U.S.A. **107**, 1059 (2010).

[14] X. Wang, J. Ren, Q. Gao, Z. Hu, Y. Sun, X. Li, D. J. Rowlands, W. Yin, J. Wang, D. I. Stuart *et al.*, Hepatitis a virus and the origins of picornaviruses, Nature (London) **517**, 85 (2015).

[15] J. A. Hadden, J. R. Perilla, C. J. Schlicksup, B. Venkatakrishnan, A. Zlotnick, and K. Schulten, All-atom molecular dynamics of the hbv capsid reveals insights into biological function and cryo-em resolution limits, eLife **7**, e32478 (2018).

[16] B. Kaufmann, A. A. Simpson, and M. G. Rossmann, The structure of human parvovirus b19, Proc. Natl. Acad. Sci. U.S.A. **101**, 11628 (2004).

[17] L. Filion and M. Dijkstra, Prediction of binary hard-sphere crystal structures, Phys. Rev. E **79**, 046714 (2009).

[18] G. J. Pauschenwein and G. Kahl, Clusters, columns, and lamellae—minimum energy configurations in core softened potentials, Soft Matter **4**, 1396 (2008).

[19] J. Dobnikar, J. Fornleitner, and G. Kahl, Ground states of model core-softened colloids, J. Phys. Condens. Matter **20**, 494220 (2008).

[20] K. Müller, N. Osterman, D. Babic, C. N. Likos, J. Dobnikar, and A. Nikoubashman, Pattern formation and coarse-graining in two-dimensional colloids driven by multiaxial magnetic fields, Langmuir **30**, 5088 (2014).
[21] J. Qin, G. S. Khaira, Y. Su, G. P. Garner, M. Miskin, H. M. Jaeger, and J. J. de Pablo, Evolutionary pattern design for copolymer directed self-assembly, Soft Matter **9**, 11467 (2013).
[22] S. Kriegman, D. Blackiston, M. Levin, and J. Bongard, A scalable pipeline for designing reconfigurable organisms, Proc. Natl. Acad. Sci. U.S.A. **117**, 1853 (2020).
[23] B. Srinivasan, T. Vo, Y. Zhang, O. Gang, S. Kumar, and V. Venkatasubramanian, Designing dna-grafted particles that self-assemble into desired crystalline structures using the genetic algorithm, Proc. Natl. Acad. Sci. U.S.A. **110**, 18431 (2013).
[24] M. Z. Miskin and H. M. Jaeger, Adapting granular materials through artificial evolution, Nat. Mater. **12**, 326 (2013).
[25] R. Vácha, F. J. Martinez-Veracoechea, and D. Frenkel, Receptor-mediated endocytosis of nanoparticles of various shapes, Nano Lett. **11**, 5391 (2011).
[26] K. Xiong, J. Zhao, D. Yang, Q. Cheng, J. Wang, and H. Ji, Cooperative wrapping of nanoparticles of various sizes and shapes by lipid membranes, Soft Matter **13**, 4644 (2017).
[27] D. R. Elias, A. Poloukhtine, V. Popik, and A. Tsourkas, Effect of ligand density, receptor density, and nanoparticle size on cell targeting, Nanomedicine **9**, 194 (2013).
[28] V. Schubertová, F. J. Martinez-Veracoechea, and R. Vácha, Influence of ligand distribution on uptake efficiency, Soft Matter **11**, 2726 (2015).